

Ferroelectric polarization gating MoS₂ photodetector

Xudong Wang^{1,†}, Jianlu Wang^{1,*}, Peng Wang¹, Weida Hu^{1,*}, Xiaohao Zhou¹, Nan Guo¹, Shuo Sun¹, Hong Shen¹, Tie Lin¹, Minghua Tang², Lei Liao³, Anquan Jiang⁴, Jinglan Sun¹, Xiangjian Meng¹, Xiaoshuang Chen¹, Wei Lu¹, Junhao Chu¹

¹National Laboratory for Infrared Physics, Shanghai Institute of Technical Physics, Chinese Academy of Sciences, 500Yu Tian Road, Shanghai 200083, China

²School of Materials Science and Engineering, Xiangtan University, Xiangtan, Hunan 411105, China

³Department of Physics and Key Laboratory of Artificial Micro- and Nano-Structures of Ministry of Education, Wuhan University, Wuhan 430072, China

⁴Department of Microelectronics, Fudan University, 220 Handan Road, Shanghai 200433, China

Abstract: Recent research on two dimensional (2D) materials, such as graphene¹, MoS₂², etc., has revealed their prospective applications in future electronic/optoelectronic devices³⁻⁹. High-performance MoS₂ photodetectors have been fabricated¹⁰⁻¹³. However, the ratio of photoresponse current to dark current, a figure of merit for a photodetector, is still very small even under high gate and source-drain bias. Here we demonstrate a ferroelectric polarization gating MoS₂ photodetector with a poly(vinylidene fluoride-trifluoroethylene) ferroelectric layer in place of oxide layer in a traditional field effect transistor. The dark current of the photodetector is strongly suppressed by the ferroelectric polarization. A high ratio of photoresponse current to dark current, up to $\sim 10^4$, has been achieved with a response time ~ 1.8 ms at wavelengths of 500-800 nm under 0.1-1V source-drain bias and ZERO gate bias. Most strikingly, such a hybrid structure of ferroelectric and photoelectric 2D materials decreases the band gap of few-layer MoS₂ from typical 1.2~1.8 eV to ~ 0.6 eV due to the ultra-high electrostatic field from the ferroelectric polarization. With this characteristic, photoresponse wavelengths of the photodetector are extended to infrared (0.85-1.55 μ m) for the first time. Such MoS₂ photodetector with a hybrid of ferroelectrics and photoelectrics may lead to a disruptive revolution in prospective 2D electronic/optoelectronic devices.

During the past ten years, because of the unique properties of single layer graphene, two dimensional (2D) materials draw more and more attention for their potential applications in future nanoscale electronic/optoelectronic devices¹⁻⁹. Molybdenum disulfide (MoS_2), consisting of layered S-Mo-S units structure bonded by van der Waals, have also been widely studied in recent years^{2, 8-13}. The MoS_2 is a typical semiconductor with a band gap range from 1.2eV to 1.8eV as the thickness decreases from bulk to monolayer¹⁴⁻¹⁶. Field effect transistors based on monolayer or multilayer MoS_2 possess high current ON/OFF ratios of up to 10^7 - 10^8 ^{8, 17-19}. Owing to these special features, ultrathin MoS_2 becomes a promising candidate material for future electronic applications.

For transistors based on 2D graphene and MoS_2 , traditional dielectric materials, such as SiO_2 , HfO_2 , and Al_2O_3 , with linear dielectric response to an electric field, are usually selected as gate dielectrics^{1,8,10,12,13}. Many interesting and meaningful physical properties have been discovered using these materials. Among these, the optoelectronic properties of a field effect transistor, especially the MoS_2 photodetector (sometimes named a phototransistor) have attracted intensive attention¹⁰⁻¹³. For these photodetectors, additional gate bias (V_g) and a large drain-source bias (V_{sd}) are essential for obtaining high sensitivity. Such V_g may induce a leakage between source and gate, and the large V_{sd} leads to a significant increase in dark current between the source and drain, as well as a self-heating effect in the channel. These effects will not only cause a large power dissipation, but will also seriously degrade the performance, such as resulting in a very low ratio of photoresponse current to dark current^{20, 21}. In recent

years, poly(vinylidene fluoride-trifluoroethylene) (P(VDF-TrFE)) ferroelectric polymer film has been used in nano electronic devices, such as nonvolatile memories²²⁻²⁵. In these devices, the function of ferroelectric film is to tune the transport properties of the channel. However, ferroelectric materials combined with the photoelectric 2D materials have never been used for optoelectronic devices, for example photodetectors.

In this work, the MoS₂ transistor with a ferroelectric gate is used as a photodetector, wherein the few-layer MoS₂ serves as the photosensitive semiconducting channel while the remnant polarization of P(VDF-TrFE) is employed to depress the dark current of the MoS₂ semiconducting channel. The stable remnant polarization can provide an ultra-high local electrostatic field ($\sim 10^9$ V/m within a several nanometer scale) in the semiconductor channel which is larger than that produced by gate bias in traditional field effect transistors¹¹⁻¹³. With such an ultra-high electrostatic field, the few-layer MoS₂ channel is maintained at a fully depleted state, significantly increasing the ratio of photoresponse current to dark current to a value of 10^3 - 10^5 at ZERO gate voltage. With this characteristic, for the first time the photoresponse wavelengths of the ferroelectric polarization gating MoS₂ photodetector are extended from the visible to infrared (0.85-1.55 μ m).

A few-layer MoS₂ on a degenerately doped silicon substrate covered with 285 nm thick silicon oxide was prepared using the Scotch® tape-based mechanical exfoliation method^{2, 8}. The few-layer MoS₂ optical image with source and drain chromium (Cr, 5nm)/gold (Au, 30nm) electrodes prepared using the tape lift-off method is shown in Fig.1a. The following step was coating the P(VDF-TrFE) (70:30 in mol%) film as the

top gate, then the ultrathin semi-transparent aluminum (~ 20 nm) electrodes were deposited (shown in Fig.1b). The thickness of the few-layer MoS₂ was confirmed by the Raman spectrum (Fig.1c). The peak location of E_{2g}^1 and A_{1g} are 381.32 cm^{-1} and 404.65 cm^{-1} , respectively, and the frequency difference between E_{2g}^1 and A_{1g} vibration modes is 23.27 cm^{-1} . These data correspond to a film thickness of 2.1nm for the triple-layer MoS₂^{14,15}. The molecular configurations of MoS₂ and P(VDF-TrFE) are shown in Fig. 1d and Fig. 1e, respectively. The ferroelectric dipole direction in the P(VDF-TrFE) chain is also shown in Fig.1e. The 3D device structure schematic view of the ferroelectric polarization gating MoS₂ photodetector with the laser beam illumination is shown in Fig.1f.

Analysis continues with the ferroelectric properties of the P(VDF/TrFE) copolymer being characterized. A typical hysteresis loop for a P(VDF/TrFE) capacitor is shown in Fig.2a. The thickness of the P(VDF/TrFE) layer is 300 nm. The coercive voltage is approximately 22.5 V and the remnant polarization value is $7\text{ }\mu\text{C}/\text{cm}^2$. The polarization switching voltage can be reduced to approximately 5 V with decreasing thickness of the ferroelectric layer²³. Next, the transfer curves $I_{sd}-V_{tg}$ (drain-source current I_{sd} as a function of top gate voltage V_{tg}) of the MoS₂ transistor with ferroelectric polymer were investigated at room temperature (shown in Fig.2b). The large memory window ($\approx 30\text{V}$) in I - V curves between the voltage rise and decrease is related to the ferroelectric polarization switch process. It is more obvious by comparing this curve with the one obtained with the SiO₂ back gate (inset of Fig. 2b). A mobility of $\mu \approx 3.4\text{ cm}^2\text{V}^{-1}\text{s}^{-1}$ is calculated from the polymer gated transfer curve using the method in Ref. [8]. The

measured transfer characteristics exhibit a typical n type channel FET, showing good agreement with a conventional transistor⁸. With the back gate, a mobility of $\mu \approx 25.9 \text{ cm}^2 \text{ V}^{-1} \text{ s}^{-1}$ for the few-layer MoS₂ was obtained. The difference in the mobility derived from top or back gates maybe associated with the interface nature and the Schottky barrier at the contacts^{26,27}. Based on the ferroelectric polymer/MoS₂ structure, we can achieve three different states: P(VDF/TrFE) without polarization (named as the “fresh” state), polarization up state (P_{up}) and polarization down state (P_{down}). The P_{up} and P_{down} states are achieved by poling P(VDF-TrFE) with -50V and +50V. The $V_{\text{sd}}-I_{\text{sd}}$ characteristics (without additional gate voltage and light illumination) of these three states are shown in Fig. 2c. In P_{up} state, I_{sd} is the lowest compared to that of the other two states. This situation means that the depleted state of carriers in the MoS₂ channel is caused by the electrostatic field derived from the remnant polarization of P(VDF-TrFE). On the other hand, the P_{down} state corresponds to the accumulated states of carriers in the MoS₂ channel. The cross section of the device structures and equilibrium band diagrams at the different states are shown in Figs. 2d-2f. For a photodetector, the $V_{\text{sd}}-I_{\text{sd}}$ represents the dark current level without light illumination.

Next, the photoresponse of the MoS₂ photodetector was measured at a ZERO gate voltage. The photo switching properties (under $V_{\text{sd}} = 100 \text{ mV}$) at a wavelength of 635 nm with the three states described above are shown in Fig. 3a. In the fresh state, the ratio of photoresponse current (I_{ph}) to dark current (I_{dark}) is very small. In the P_{up} state, an I_{ph} to I_{dark} ratio of nearly 10^3 is obtained, as can be seen from the photoresponse to pulsed laser illumination curves. In the P_{down} state, I_{ph} cannot be distinguished from the

large I_{dark} as the large thermionic and drift/diffusion currents dominate channel current. The results indicate that the electrostatic field produced by the surface charge at the domain surface of P(VDF-TrFE) is strong enough to cause total depletion/accumulation of carriers in the MoS₂ semiconducting channel. The domain direction in the ferroelectric material of a charge insufficiently compensated system can be altered by a depolarization field, which leads to the random distribution of ferroelectric domains and, eventually, to the malfunction of the device. (Indeed, before fabricating the ferroelectric layer, we have characterized the photoresponse properties of back gated MoS₂ photodetector, **as shown in Figure S1**. The performance of the traditional back-gate photodetector is very poor compared to the MoS₂ photodetector with ferroelectric polarization gating.) For the following measurement, the ferroelectric polarization in P(VDF-TrFE) was preset at a P_{up} state by a short bias pulse of -50V on the top gate. The $I_{\text{sd}}-V_{\text{sd}}$ for different illumination powers at a wavelength of 635 nm is shown in Fig. 3b. The $I_{\text{sd}}-V_{\text{sd}}$ curves, as shown in Fig.3b, are nonlinear and asymmetric, indicating imperfect Ohmic contact. Figure 3c shows the laser power dependence of I_{ph} of the device with $V_{\text{sd}}=100$ mV. The inset in Fig.3c is the ratio of I_{ph} to I_{dark} for light on and light off (dark states) at different illumination powers. It can be seen that the device is very sensitive to illumination power. The responsivity (R) of the photodetector is about 3.6 A/W. The data are extracted from Fig.3b, where $V_{\text{sd}}=1$ V and $P= 100$ nW, given by $R = I_{\text{ph}} / P$, where I_{ph} is the photo current in a detector and P is the illumination power^{28,}
²⁹. The value of R (3.6A/W) is similar to Oriol Lopez-Sanchez's result ~ 40 A/W (100nW, $V_{\text{sd}}=8$ V, and $V_{\text{g}}= -70$ V)⁸. Note that, if a highly transparent electrode is chosen,

a higher responsivity can be expected. Currently, the transmittance of the available semitransparent Al electrode is only 3% for our device. The photo-induced current in Fig. 3b also shows a small nonlinear dependence on the bias voltage, which is related to the imperfect Ohmic contact. It suggests that a flawless device fabrication is needed for superior performance in the future.

In addition to the superior ratio of photoresponse current to dark current and good photo-responsivity, we conducted time-resolved photoresponse experiments by periodically turning the illuminating laser on and off at a frequency of 0.5 Hz and recorded the response signal from a high speed oscilloscope (**shown in Fig. S2**). Figure 3e shows a complete on/off circle in which the photocurrent exhibits rapid rise/fall and reaches a steady saturation. The rising and falling edges of the response current are perfectly fitted by a single exponential function. The rise (τ_r) and decay (τ_f) time of the photocurrent, is ~1.8ms and ~2ms, respectively, which is relatively fast for state-of-the-art 2D photoconductive photodetectors. In our case, the improvement of response time maybe result from the interface of P(VDF-TrFE) and MoS₂, the surface trap state of MoS₂ may be encapsulated or passivated by the fluorine or hydrogen atoms from polarized P(VDF-TrFE). Furthermore, the signals recorded by the oscilloscope remain nearly unchanged after 90, 000 cycles of operation (as shown in Fig. 3d), pointing to the excellent stability and reliability of the photodetectors. The stability of the photo-switching behavior is related to the ferroelectric polarization stability of the P(VDF-TrFE) top gate^{30, 31} and the reliability of the P(VDF-TrFE)-passivated MoS₂ channel.

All the prominent properties of our photodetector benefit from the ferroelectric-

polarization-induced ultra-high electrostatic field of the P(VDF-TrFE). The local electric field at the interface between P(VDF-TrFE) and MoS₂ layers can be estimated from $\sigma = \epsilon \epsilon_0 E$, where σ is the charge density at the surface of P(VDF-TrFE) film, which is related to the remnant polarization (P_r) of the ferroelectric materials²³, ϵ is the dielectric constant of material (the dielectric constant of MoS₂ is approximately 4-6^{32, 33}, ϵ_0 is the vacuum permittivity, E is the electric field strength, and P_r is approximately 7.0 $\mu\text{C}/\text{cm}^2$ calibrated from Fig. 2a. The calculated electric field applied to the triple-layer MoS₂ is about $0.5 \times 10^9 \text{ V/m}$. It is very difficult to obtain such an ultra-high electric field for conventional FETs as described by Naber et al.²³.

The typical photoresponse spectra of MoS₂ photodetector is from visible to near infrared (0.85 μm) as the band gap of MoS₂ ranges from 1.2 eV to 1.8 eV. As reported by Oriol Lopez-Sanchez *et al.*, photoresponse is negligible at wavelengths longer than 680 nm (corresponding to one photon energy 1.8 eV) for monolayer MoS₂¹⁰. For triple-layer MoS₂, the broad absorption tail corresponding to the indirect band transition extends to near 0.85 μm , which is in good agreement with the theoretical prediction¹³. A wider spectral response for a photodetector is important and meaningful. Therefore the response of the detector to light with long wavelength was investigated. The photoresponse of the detector to pulsed laser illumination with different wavelengths is shown in Fig 4a. Surprisingly, it is found that there is still appreciable optical current response to light with wavelength up to 1.55 μm . For the first time, our work broadens the detection of a MoS₂ photodetector from 0.85 μm (1.2 eV) to 1.55 μm (0.8 eV), even smaller than the indirect bandgap of bulk MoS₂ $\sim 1.2 \text{ eV}$.

To confirm the effect of polarization electrical field on the band structure of few-layer MoS₂, we carried out micro-photoluminescence (PL) measurements on the fresh (ferroelectric domain random) and poled (domain aligned) samples (shown in Fig.4b). The PL emission for the pole sample is red-shifted compared to the fresh sample, independent of the polarization directions. Similarly, the indirect bandgap of MoS₂ can be tuned by the external strain and confirmed by PL spectrum³⁴⁻³⁶. Note that the PL measures an optical bandgap, and is different from the bandgap from electron transport due to the exciton binding energy. In fact, the function of the strong electrical field does more than this. It has been theoretical predicted that the energy gap of the bi-layer MoS₂ can be tuned by the external electric field^{37,38}. The change of band-gap in triple-layer MoS₂ under external electric fields applied perpendicular to the layers was also calculated using the density functional theory. The band structure of triple-layer MoS₂ as a function of applied different external electric field is shown in Figs.4c-e. The indirect bandgap is reduced with an increase of the applied electric field. For example, a 0.40 V/nm of electric field strength can reduce the band gap from 1.09 to 0.71 eV. **(Details of the calculation are shown in supplementary information).**

Further studies are needed to clarify the fundamental physics principles of the ferroelectric polarization tuning for the bandgap of few-layer MoS₂. Nevertheless, the ferroelectric/MoS₂ hybrid structure photodetector shows an outstanding performance for photo detecting. The photodetector based on the same structure as 4-layer MoS₂ shows similar electronic and photoresponse properties (**shown in Fig. S3 and S4**). Our photodetector shows a high sensitivity under weak illumination, such as fluorescent

lamp (**Mov.S1**), demonstrating that the few-layer MoS₂ is very promising for a visible to near-infrared digital camera.

In summary, we have fabricated the ferroelectric polymer film gated triple-layer MoS₂. The MoS₂ device exhibited outstanding photodetection capabilities compared to traditional MoS₂ FET photodetectors. The device exhibits a high ratio of photoresponse current to dark current, broad spectral regions detection, stable and fast photoresponse, and is superior to recently reported MoS₂ photodetectors. The infrared (0.85-1.55 μm) photoresponse of the ferroelectric polarization gating MoS₂ photodetector suggests that such a MoS₂ photodetector is very promising for use in optical communications. The energy gap engineering of a 2D material system combined with an ultra-high ferroelectric-polarization-induced electrostatic field is an attractive research area for next-generation high performance 2D electronic/optoelectronic devices. There are many fruitful and fundamental physics issues in ferroelectric/photoelectric 2D material hybrid systems to be explored in future studies.

Fabrication of the MoS₂ photodetectors.

All measurements were performed under ambient conditions. Triple layers of MoS₂ were exfoliated from commercially available crystals of molybdenite (SPI Supplies brand Moly Disulfide) using the Scotch®-tape micromechanical cleavage technique pioneered for the production of graphene. Triple layers of MoS₂ were deposited on a ~285 nm thick SiO₂ dielectric layer on top of a highly-doped p-type Si wafer (resistivity $<5 \times 10^{-3} \Omega \cdot \text{cm}$). Electrical contacts were patterned on top of MoS₂ flakes using a conventional lift-off technique. Cr (5 nm) and Au (50 nm) electrodes were deposited by thermal evaporation at room temperature. The device was then annealed at 200 °C in a vacuum tube furnace for 2 hours (100 sccm Ar) to remove resist residue and to decrease contact resistance. Then the top gate P(VDF-TrFE)(70:30 mol%) films were prepared by spin coating on the top of the MoS₂. Finally, ultrathin alumina films were deposited by thermal evaporation as the top gate semi-transparent electrodes.

Characterization of the photodetectors

We performed the electrical and optoelectrical characterization of our device at room temperature using a Lake Shore probe station and Agilent semiconductor parameter analyzer.

In this work, electrical measurements were carried out using an Agilent B2902A, Signal Recovery current preamplifier, lock-in amplifier Signal Recovery 7270 and a current preamplifier Signal Recovery 5182 on the Lake Shore probe station. The photoresponse to laser excitation used a focused $\lambda=500\text{-}1550\text{nm}$ laser beam. A monochromator was used for wavelength-dependent measurements of the photocurrent.

The Raman spectra and PL spectra were acquired by the Lab Ram HR800 from HORIBA.

Reference

1. Novoselov, K. S. *et al.* Electric field effect in atomically thin carbon films. *Science* **306**, 666–669 (2004).
2. Novoselov, K. S. *et al.* Two-dimensional atomic crystals. *Proc. Natl. Acad. Sci. USA* **102**, 10451–10453 (2005).
3. Nathaniel M. G. *et al.* Hot Carrier–Assisted Intrinsic Photoresponse in Graphene. *Science* **334**, 648 (2011).
4. Xia, F. *et al.* Ultra-fast graphene photodetector. *Nature Nanotech.* **4**, 839–843 (2009).
5. Williams J. R. *et al.* Quantum Hall Effect in a Gate-Controlled p-n Junction of Graphene. *Science* **317**, 638 (2007).
6. Yang H. J. *et al.* Graphene Barristor a Triode Device with a Gate-Controlled Schottky Barrier. *Science* **336**, 1140 (2012).
7. Britnell L. *et al.* Field-Effect Tunneling Transistor Based on Vertical Graphene Heterostructures. *Science* **335**, 947 (2012).
8. Radisavljevic, B. *et al.* Single-layer MoS₂ transistors. *Nature Nanotech.* **6**, 147–150 (2011).
9. Grigorenko, A. N. *et al.* Graphene plasmonics. *Nature Photon.* **6**, 749 (2012).
10. Lopez-Sanchez, O. *et al.* Ultrasensitive photodetectors based on monolayer MoS₂. *Nature Nanotech.* **8**, 497–501 (2013).
11. Yin, Z. *et al.* Single-layer MoS₂ phototransistors. *ACS Nano* **6**, 74–80 (2011).
12. Lee, H. S., *et al.* MoS₂ Nanosheet Phototransistors with Thickness-Modulated Optical Energy Gap. *Nano Lett.* **12**, 3695–3700 (2012).
13. Choi, W. *et al.* High-detectivity multilayer MoS₂ phototransistors with spectral response from ultraviolet to infrared. *Adv. Mater.* **24**, 5832–5836 (2012).
14. Mak, K. F. *et al.* Atomically thin MoS₂: a new direct-gap semiconductor. *Phys. Rev. Lett.* **105**, 136805 (2010).
15. Lee, C. *et al.* Anomalous Lattice Vibrations of Single and Few-Layer MoS₂. *ACS Nano* **4**, 2695–2700 (2010).
16. Ganatra, R. *et al.* Few-Layer MoS₂: A Promising Layered Semiconductor, *ACS Nano* **8**, 4074–4099 (2014).
17. Liu, H. *et al.* Channel length scaling of MoS₂ MOSFETs. *ACS Nano* **6**, 8563–8569 (2012).
18. Bertolazzi, S. *et al.* Nonvolatile Memory Cells Based on MoS₂/Graphene Heterostructures. *ACS Nano* **7**, 3246–3252 (2013).
19. Qiu, H. *et al.* Electrical characterization of back-gated bi-layer MoS₂ field-effect transistors and the effect of ambient on their performances. *Appl. Phys. Lett.* **100**, 123104 (2012).
20. Ionescu, A. M. *et al.* Tunnel field-effect transistors as energy-efficient electronic switches, *Nature* **479**, 329–337 (2011).
21. Ouyang, Y. *et al.* Heat dissipation in carbon nanotube transistors. *Appl. Phys. Lett.* **89**, 183122 (2006).
22. Zheng, Y. *et al.* Graphene Field-Effect Transistors with Ferroelectric Gating. *Phys. Rev. Lett.* **105**, 166602 (2010).
23. Naber, R. C. G. *et al.* High-performance solution-processed polymer ferroelectric field-effect transistors. *Nature Materials* **4**, 243–248 (2005).
24. Baeumer, C. *et al.* Tunable Carrier Type and Density in Graphene/PbZr_{0.2}Ti_{0.8}O₃ Hybrid

- Structures through Ferroelectric Switching. *Nano Lett.* **13**, 1693–1698 (2013).
25. Lee, H. S. *et al.* MoS₂ Nanosheets for Top-Gate Nonvolatile Memory Transistor Channel. *Small* **8**, 3111–3115 (2012).
 26. Jena, D. *et al.* Enhancement of carrier mobility in semiconductor nanostructures by dielectric engineering. *Phys. Rev. Lett.* **98**, 136805 (2007).
 27. Fonoberov, V. A. *et al.* Giant enhancement of the carrier mobility in silicon nanowires with diamond coating. *Nano Lett.* **6**, 2442–2446 (2006).
 28. Konstantatos, G. *et al.* Nanostructured materials for photon detection. *Nature Nanotech.* **5**, 391–400 (2010).
 29. Guo, Y. *et al.* Functional Organic Field-Effect Transistors. *Adv. Mater.* **22**, 4427–4447. (2010).
 30. Kim, W. Y. *et al.* Retention Performance of Ferroelectric Polymer Film for Nonvolatile Memory Devices. *IEEE Electron Device Lett.* **30**, 822–824 (2009).
 31. Reece, T. J. *et al.* Investigation of state retention in metal–ferroelectric–insulator–semiconductor structures based on Langmuir–Blodgett copolymer films. *J. Appl. Phys.* **108**, 024109 (2010).
 32. Chen, X. *et al.* Probing the electron states and metal-insulator transition mechanisms in molybdenum disulphide vertical heterostructures. *Nature. Commun.* **6**, 6088 (2015).
 33. Santos, E. J. G. *et al.* Electrically Driven Tuning of the Dielectric Constant in MoS₂ Layers, *ACS Nano* **7**, 10741–10746 (2013).
 34. Hui, Y. Y. *et al.* Exceptional Tunability of Band Energy in a Compressively Strained Trilayer MoS₂ Sheet. *ACS Nano* **7**, 7126–7131 (2013).
 35. Conley, H. J. *et al.* Bandgap Engineering of Strained Monolayer and Bilayer MoS₂. *Nano Lett.* **13**, 3626–3630 (2013).
 36. Castellanos-Gomez, A. *et al.* Local Strain Engineering in Atomically Thin MoS₂. *Nano Lett.* **13**, 5361–5366 (2013).
 37. Ramasubramaniam, A. *et al.* Tunable band gaps in bilayer transition-metal dichalcogenides. *Phys. Rev. B* **84**, 205325 (2011).
 38. Zibouche, N. *et al.* Transition-metal dichalcogenide bilayers: Switching materials for spintronic and valleytronic applications, *Phys. Rev. B* **90**, 125440 (2014).

Acknowledgements

This work was partially supported by the Major State Basic Research Development Program (Grant No. 2013CB922302 and 2014CB921600), Natural Science Foundation of China (Grant Nos. 11374320, 11322441 and 11104301), and Fund of Shanghai Science and Technology Foundation (Grant Nos. 14JC1406400).

Author contributions

J.W and W.H conceived and supervised the research. X.W and J.W. fabricated the devices. X.W and P.W. performed the measurements. X.Z carried out the calculated part. J.W and W.H wrote the paper. All authors discussed the results and revised the manuscript.

Additional information

Supplementary information is available in the online version of the paper. Correspondence and requests for materials should be addressed to J.W. and W.H.

Competing financial interests

The authors declare no competing financial interests.

Figures

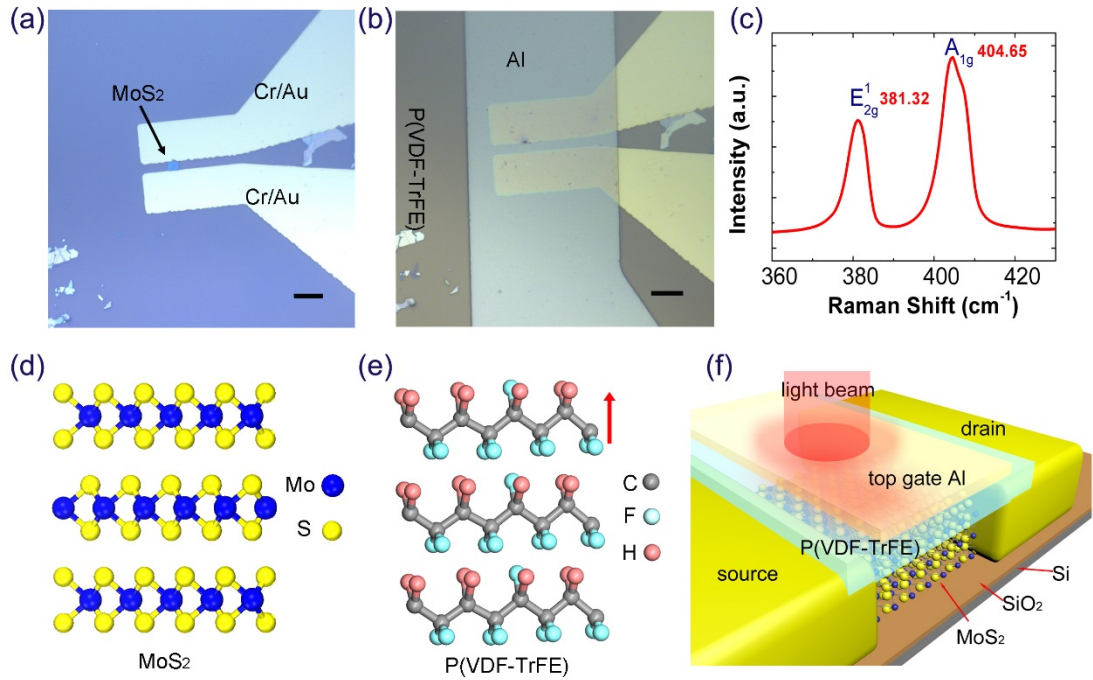


Figure 1. Fabrication and structure of few-layer MoS₂ photoetector. **a**, Optical image of the triple-layer MoS₂ on top of a silicon substrate with 285-nm-thick SiO₂ layer, with source and drain (chromium/gold, Cr/Au) electrodes. Scale bar, 10 μ m. **b**, Optical image of the whole device based on the **a**. The device is comprised of triple-layer MoS₂ with Cr/Au contract, 300 nm P(VDF-TrFE) ferroelectric polymer and semi-transparent aluminum top electrode. Scale bar, 10 μ m. **c**, The Raman spectra of triple layer MoS₂. The peak position of the E_{2g}^1 and A_{1g} are 381.32 cm⁻¹ and 404.65 cm⁻¹, respectively. The separation between E_{2g}^1 and A_{1g} modes is about 23.27 cm⁻¹. **d**, Schematic structure of triple-layer MoS₂. **e**, Schematic structure of P(VDF-TrFE) ferroelectric polymer. The polarization direction of the polymer is pointed out by arrow. **f**, Three dimensional schematic view of the triple-layer MoS₂ photodetector with monochromatic light beam.

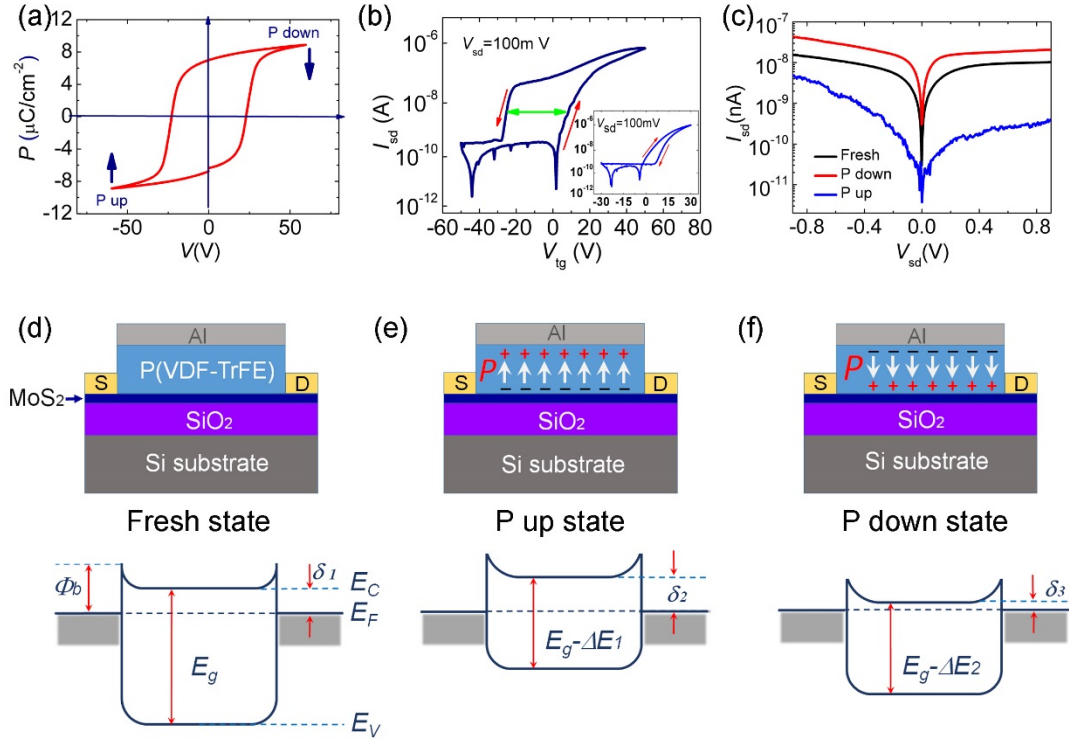


Figure 2. Ferroelectric polarization related electric properties of the P(VDF-TrFE)/MoS₂ hybrid structure. **a**, The ferroelectric hysteresis loop 300 nm P(VDF-TrFE) film capacitor. It is measured using sawyer-Tower circuit at 1 Hz applied voltage frequency. **b**, The transfer curves of triple-layer MoS₂ channel with P(VDF-TrFE) ferroelectric polymer gate on dark state at room temperature. The transfer characteristics of triple-layer MoS₂ with SiO₂ back gate are shown in the inset. **c**, The V_{sd} - I_{sd} characteristics (at ZERO gate voltage) with three states of ferroelectric layer. The three states are; fresh state (ferroelectric layer without polarization), polarization up ("P up", polarized by a pulse V_g of -50 V) and polarization down ("P down", polarized by an pulse V_g of -50 V) states, respectively. **d-f**, The cross section structures of the device and equilibrium energy band diagrams of three different ferroelectric polarization states without applied V_{sd} . For the band diagrams of different states, small

Schottky barriers at the contacts of source and drain electrode with the MoS₂ channel are considered. E_F , E_c , E_v , Φ_B , and E_g are the Fermi level energy, minimum conduction band energy, maximum valence band energy, Schottky barrier height and bandgap of MoS₂, respectively. δ is the height from bottom of conduction to the Fermi level. The δ_1 , δ_2 and δ_3 are relate to the three states.

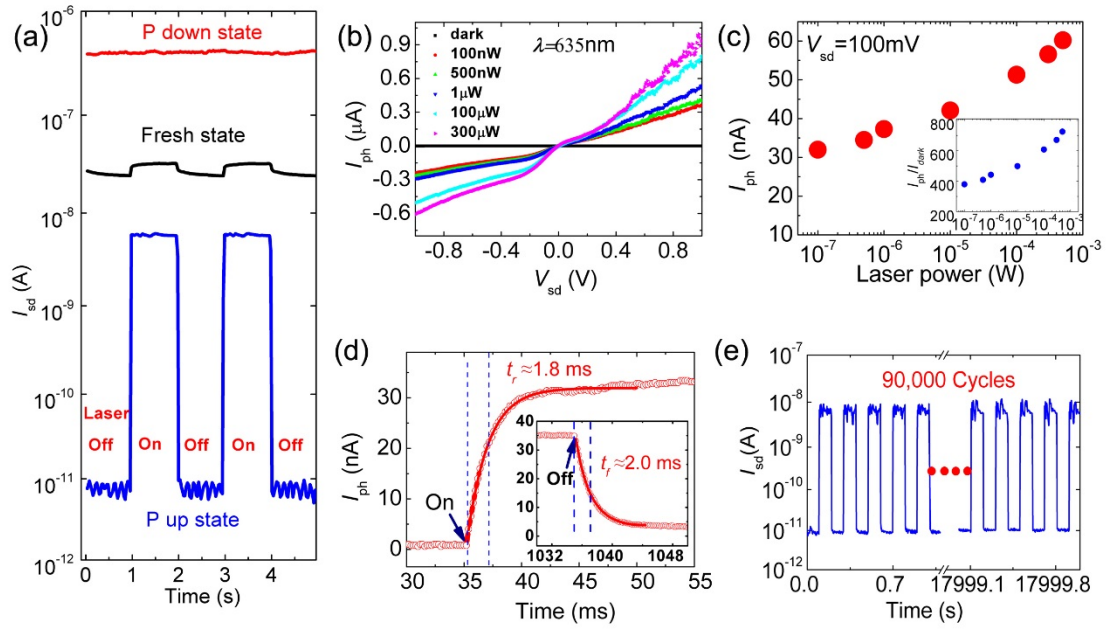


Figure 3. Photoresponse properties of the ferroelectric polarization gating triple-layer MoS₂ photodetector. **a**, Photoswitching behavior of ferroelectric polarization gating triple-layer MoS₂ photodetector at three states ($\lambda=635\text{nm}$, $V_{\text{sd}}=100\text{mV}$, $P=100\text{nW}$). **b**, Drain-source characteristic of the photodetector in the dark and under different illuminating light powers. (100nW to 300μW). **c**, Dependence of photocurrent on illumination powers. Inset is the ratio of photoresponse current to dark current under different illumination powers. **d**, The rise and fall of the photocurrent and the fitted data using exponential functions.(recorded by $V_{\text{sd}}=100\text{mV}$ and $P=100\text{nW}$). **e**, Photocurrent response during 90,000 cycles of operation at $V_{\text{sd}}=100\text{mV}$ and $P=100\text{nW}$. The device shows an enduring photoresponse.

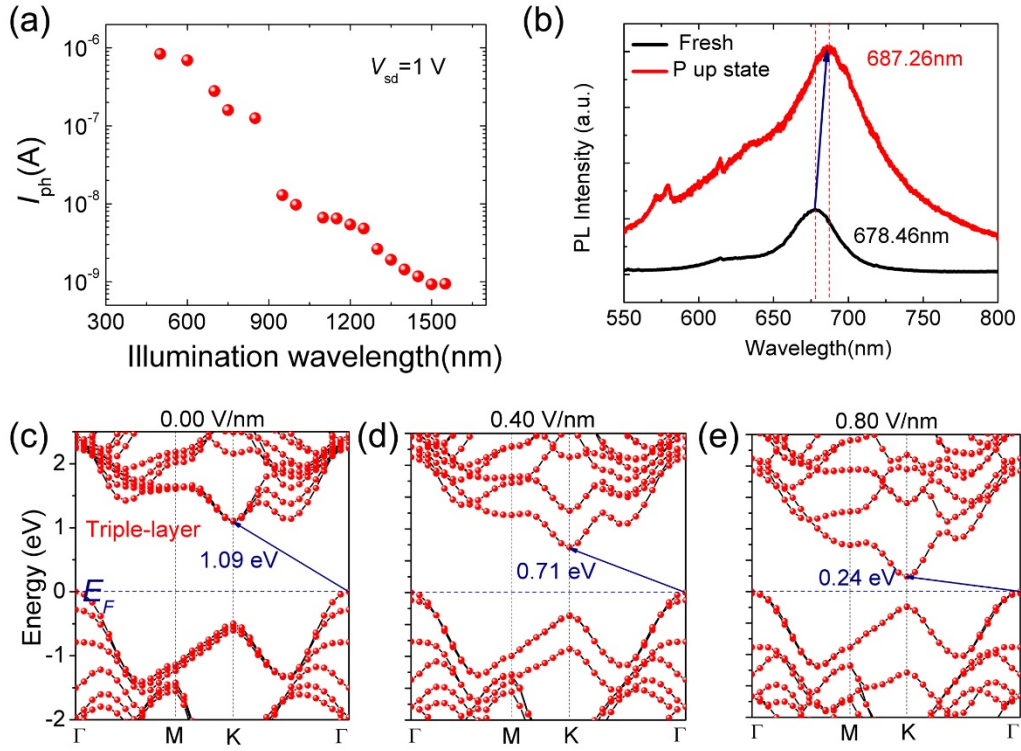


Figure 4. Infrared photoresponse of ferroelectric polarization gating few-layer MoS₂ photodetector beyond its intrinsic bandgap. a, Photocurrent of a similar triple layer MoS₂ with polarization gating as a function of light wavelength from 500 nm to 1550 nm at $V_{sd}=1$ V and $P=100\mu$ W). **b,** Comparison photoluminescence spectrum of fresh and polarization gating triple-layer MoS₂. **c-e,** The band structures evolution of triple-layer MoS₂ under different external electric field (0.0, 0.4, and 0.8 V/nm) from first-principles DFT calculation.

Supplementary Information for Ferroelectric polarization gating MoS₂ photodetector

Email: jlwang@mail.sitp.ac.cn, wdhu@mail.sitp.ac.cn

Contents

- 1. Photoresponse properties of back-gated triple-layer MoS₂ photodetector.**
- 2. Time-resolved photoresponse of ferroelectric polarization gating MoS₂ photodetector.**
- 3. Calculation details on band structures evolution of triple-layer MoS₂.**
- 4. Fabrication processing, structure and photoresponse properties of four-layer MoS₂ photodetector.**
- 5. Infrared photoresponse properties of ferroelectric polarization gating MoS₂ photodetector.**
- 6. References**

Movies:

Mov S1

1. Photoresponse properties of back-gated triple-layer MoS₂ photodetector.

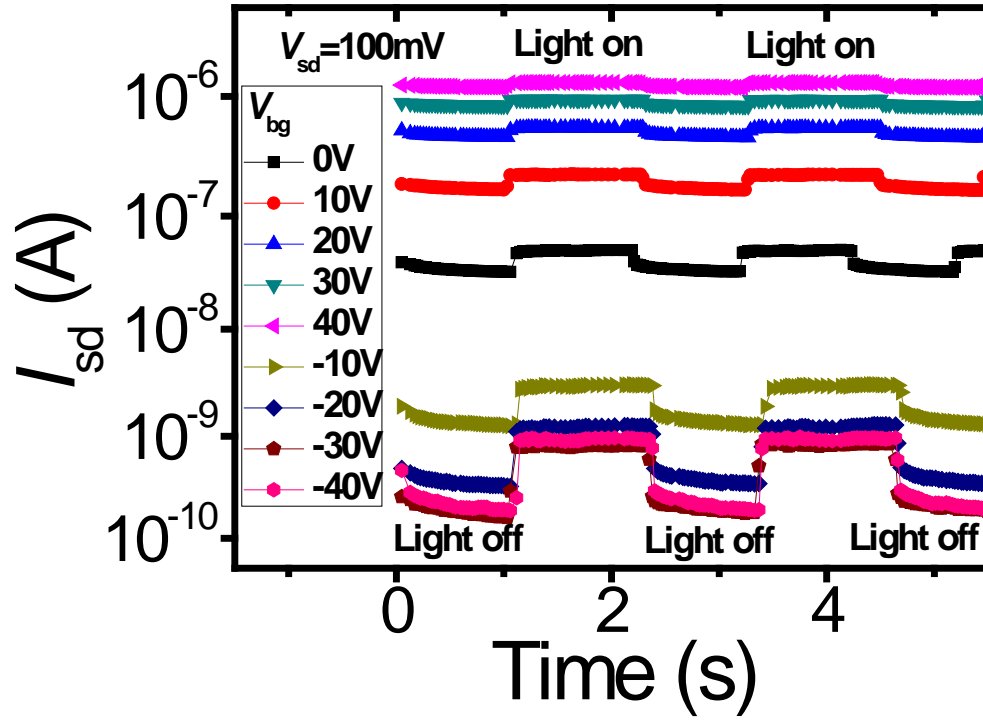


Figure S1. Photoresponse behavior of back-gated triple-layer MoS₂ photodetector with different back gate voltages under $V_{sd}=100$ mV at a wavelength of 635 nm ($P=100$ nW).

2. Time-resolved photoresponse of ferroelectric polarization gating

MoS₂ photodetector

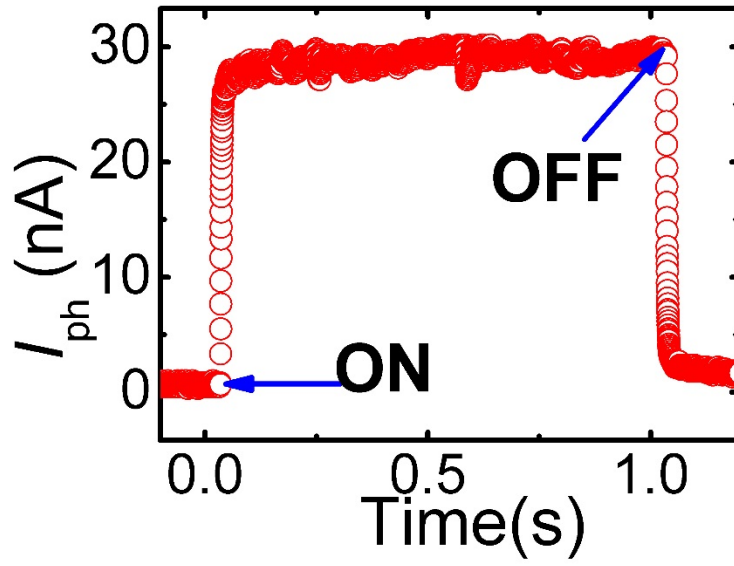


Figure S2. Time-resolved photoresponse of ferroelectric polarization gating MoS₂ photodetector. The data are recorded by a high speed oscilloscope at $V_{sd}=100\text{mV}$ and $P=100\text{nW}$.

3. Fabrication processing, structure and photoresponse properties of four-layer MoS₂ ferroelectric field effect transistor.

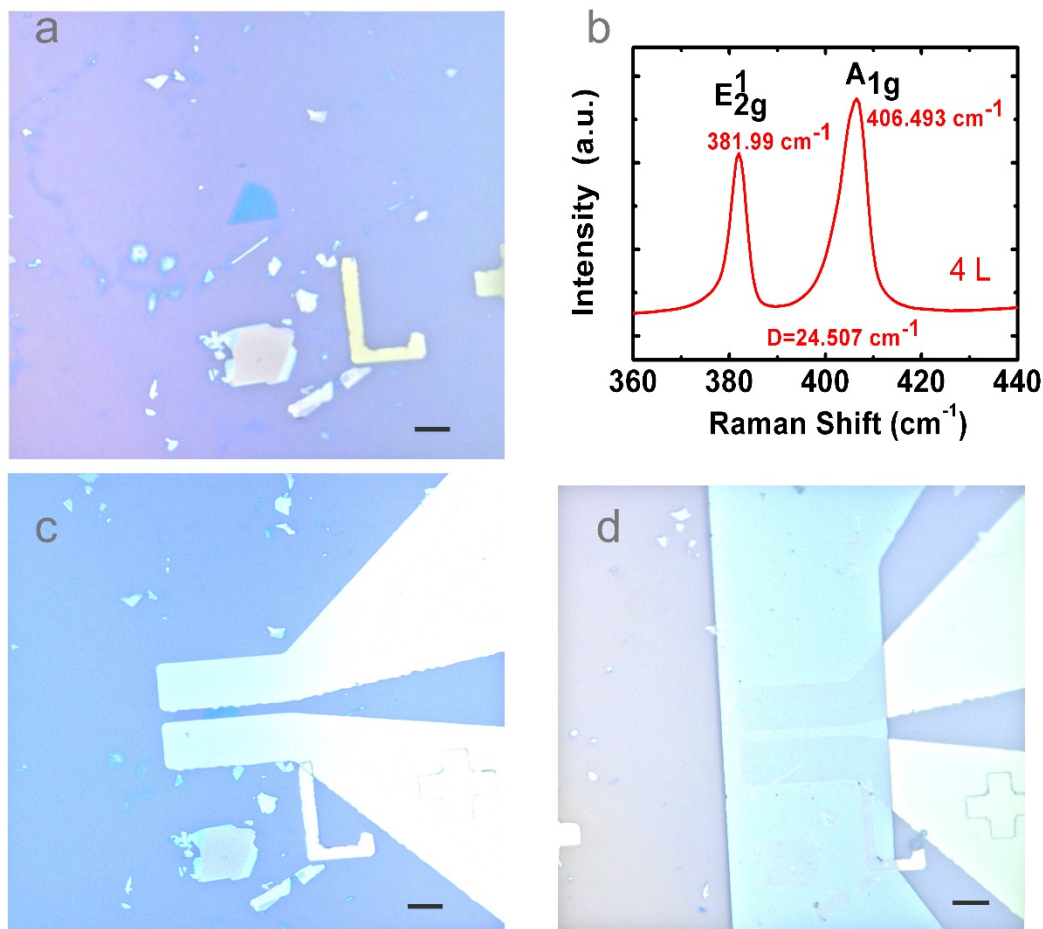


Figure S3. **Fabrication and structure of four-layer MoS₂ detector.** **a**, Optical image of the four-layer MoS₂. Scale bar, 10μm. **b**, The Raman spectra of triple-layer MoS₂. The peak position of the E_{2g}^1 and A_{1g} are 381.99 cm⁻¹ and 406.49 cm⁻¹, respectively. The separation between E_{2g}^1 and A_{1g} modes is about 24.50 cm⁻¹. **c**, Optical image of the four-layer MoS₂ on top of a silicon substrate with 285-nm-thick SiO₂ layer, with source and drain (chromium/gold, Cr/Au) electrode. Scale bar, 10μm. **d**, Optical image of the whole device based on **c**. The device is comprised of four-layer MoS₂ with Cr/Au contact, 300 nm P(VDF-TrFE) ferroelectric polymer and semi-transparent aluminum top electrode. Scale bar, 10μm.

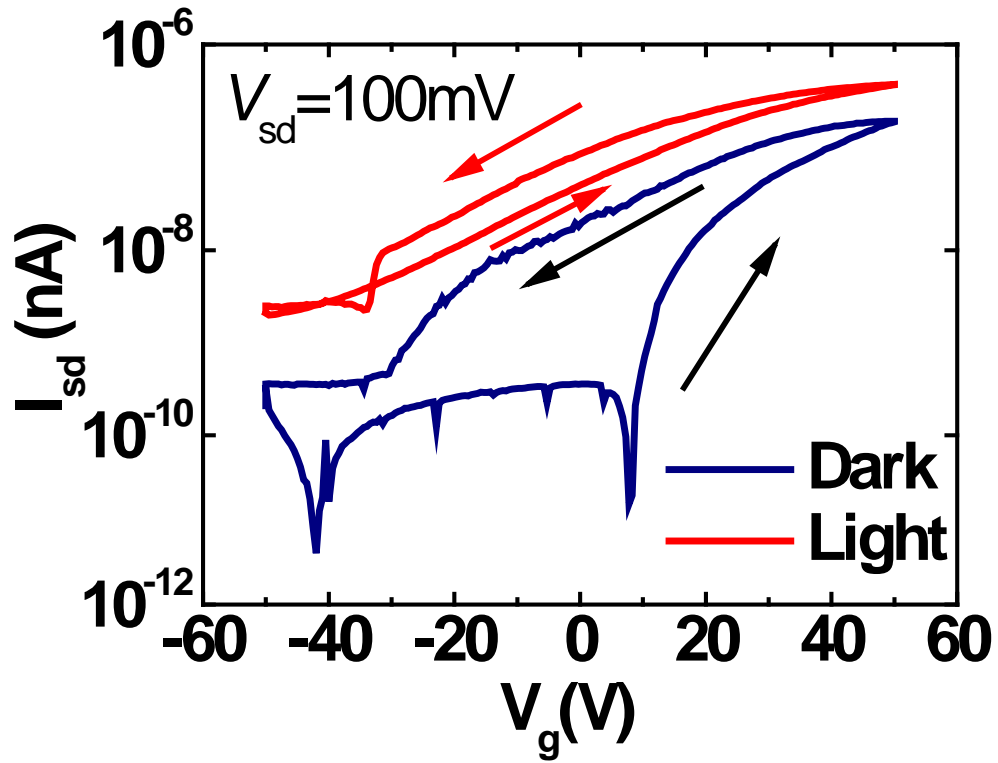


Figure S4. The transfer curves of four-layer MoS₂ photodetector in dark (red line) and light (blue line) states, respectively. The wavelength of the light illumination is 635nm.

4. Calculations on band structures evolution of triple-layer MoS₂

The first-principle DFT calculations were performed within the DMol³ code^{S1}. The generalized gradient approximation (GGA) with the Perdew–Burke–Ernzerhof (PBE) function was utilized as the exchange–correlation function^{S2}. The DFT-D (D stands for

dispersion) approach within the Grimme scheme was adopted for the vdW corrections^{S3}. DFT Semi-core Pseudopots (DSPP), which induce some degree of relativistic correction into the core, were used for the core treatment. Moreover, double numerical atomic orbital plus polarization was chosen as the basis set, with the global orbital cutoff of 4.6 Å. The k-point was set to 7x7x1 for the structural optimization and 11x11x1 for the electronic properties calculations, and the smearing value was 0.005 Ha. The convergence tolerances of energy, maximum force, and maximum displacement were set to 1.0×10^{-5} Ha, 0.002 Ha/Å and 0.005 Å respectively. The vacuum length between two adjacent images in the supercell is longer than 15 Å. The external electric field of 0 to 1.0 V/nm was applied in the direction perpendicular to the triple-layer plane, and then geometry relaxation was carried out.

Furthermore, the band gap (E_g) value as a function of electric field is displayed in Figure S6. Clearly, the value of E_g is nearly linearly dependent on electric field with the slope of 1.12. The linear relationship of E_g and electric field was also reported for transition-metal dichalcogenide bilayers under external electric field^{S4}.

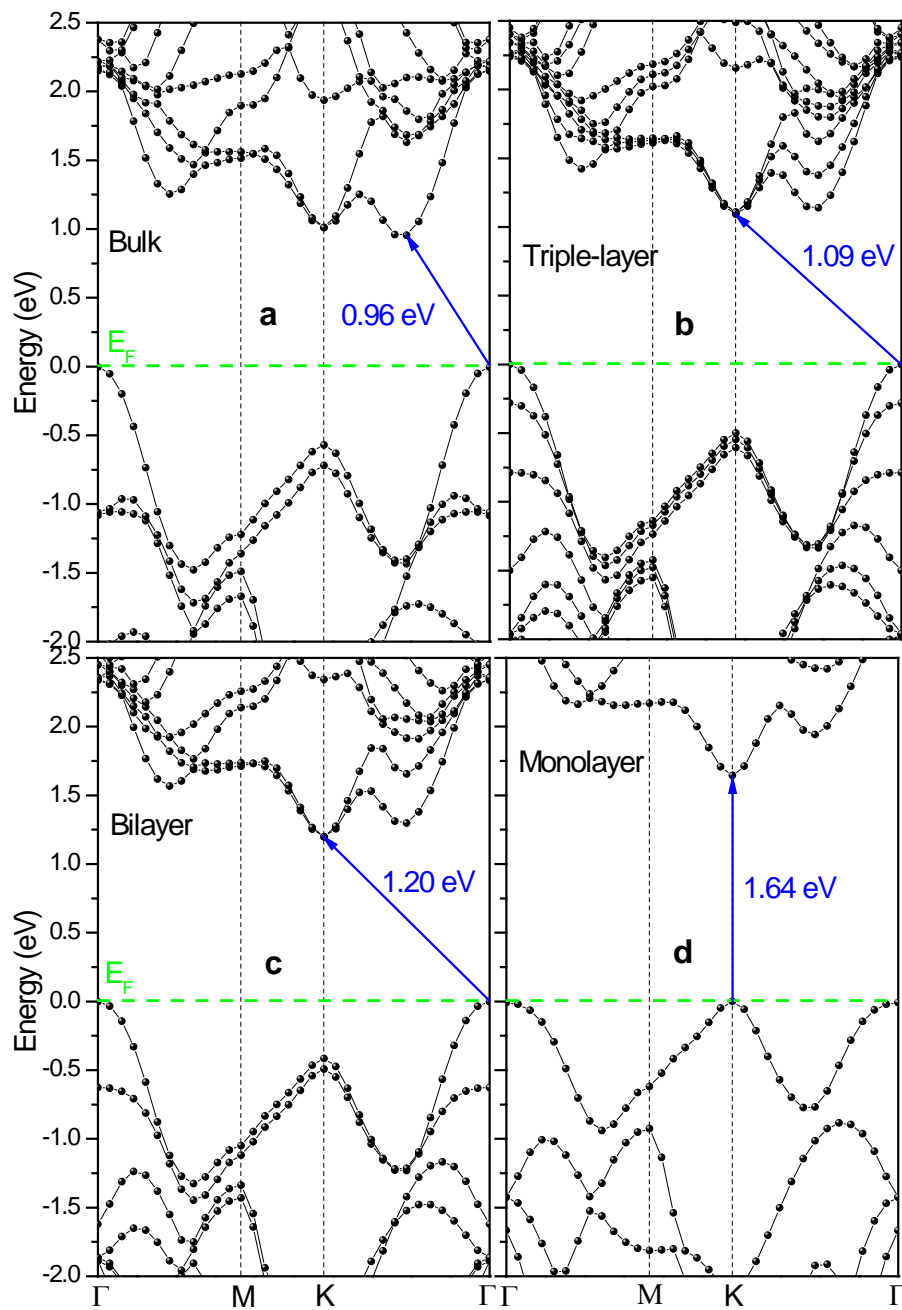


Figure S5. Computed electronic band structures of bulk (a), triple-layer (b), bilayer, and monolayer (d) MoS₂. The Fermi level (E_F) is shifted to the top of the valence band.

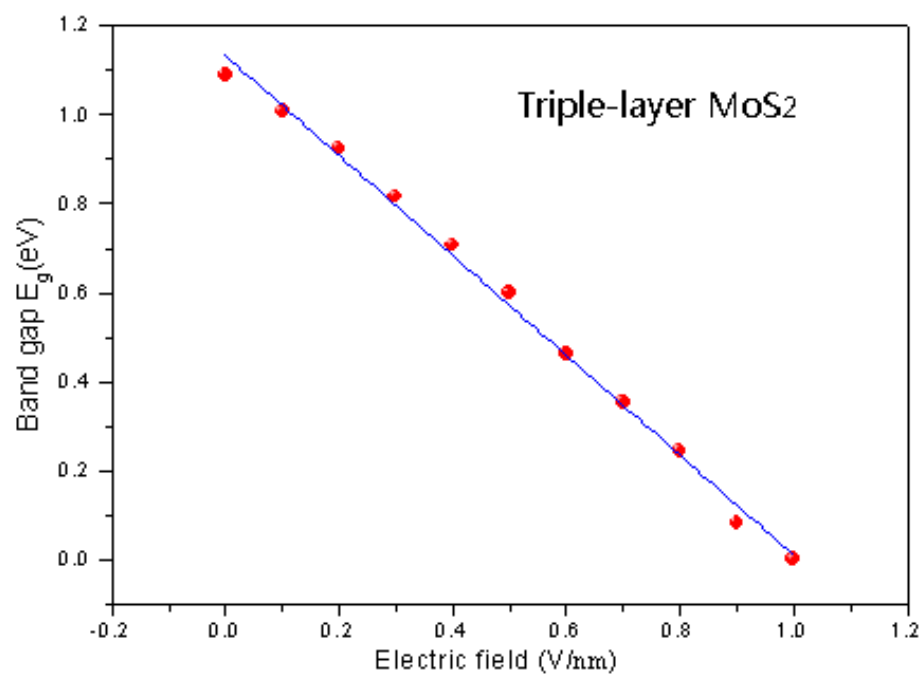


Figure S6. Band gap versus applied electric field for triple-layer MoS₂. The red (dotted) and blue (solid line) are the calculated data and fitted line, respectively.

5. Photoresponse properties of ferroelectric polarization gating MoS₂ photodetector in the infrared wavelengths

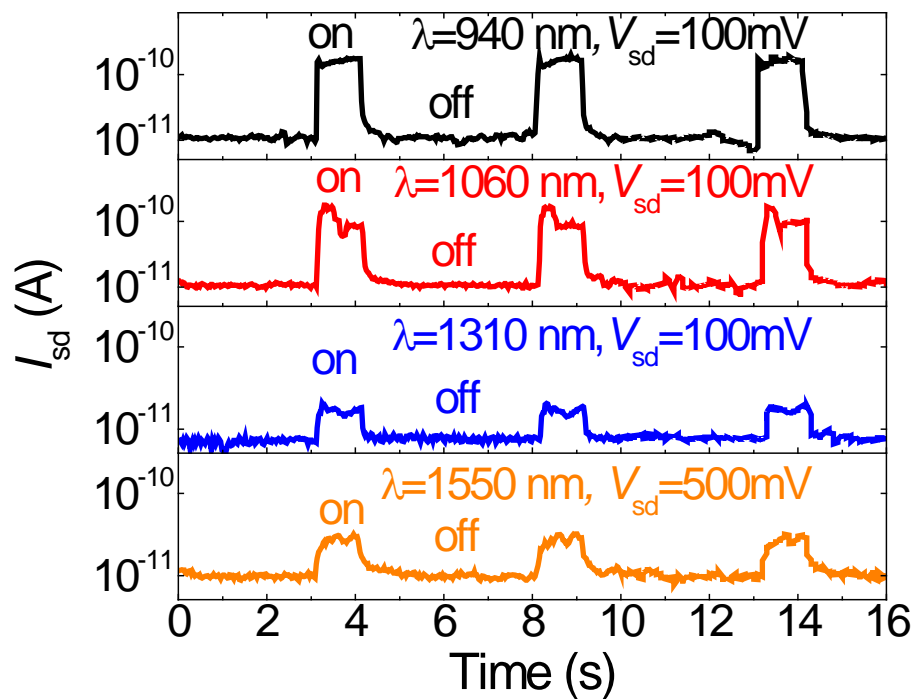


Figure S7. Infrared photoswitching behavior of ferroelectric polarization gating few-layer MoS₂ photodetector under 960 nm, 1060 nm, 1310 nm and 1550 nm wavelength laser illuminations, respectively.

6. References

- S1 B. Delley, J. Chem. Phys., 2000, **113**, 7756.
- S2 J. P. Perdew, K. Burke and M. Ernzerhof, Phys. Rev. Lett., 1996, **77**, 3865.
- S3 S. Grimme, J. Comput. Chem., 2006, **27**, 1787.
- S4 N. Zibouche, P. Philipsen, A. Kuc and T. Heine, Phys. Rev. B, 2014, **90**, 125440.

Movies

Mov S1

Photoresponse behavior of ferroelectric polarization gated few-layer MoS₂ photodetector under fluorescent lamp illumination.